

# Broadband coherent XUV light from $e^-/e^+$ microbunching in an intense laser pulse

Michael J. Quin,<sup>1,\*</sup> Antonino Di Piazza,<sup>2,3,1,†</sup> Christoph H. Keitel,<sup>1</sup> and Matteo Tamburini<sup>1,‡</sup>

<sup>1</sup>*Max-Planck-Institut für Kernphysik, Saupfercheckweg 1, 69117 Heidelberg, Germany*

<sup>2</sup>*Department of Physics and Astronomy, University of Rochester, Rochester, NY 14627, USA*

<sup>3</sup>*Laboratory for Laser Energetics, University of Rochester, Rochester, NY 14623, USA*

(Dated: November 27, 2024)

Attosecond pulses of coherent extreme ultraviolet (XUV) light are instrumental for studying sub-atomic dynamics, and are often produced from a free electron laser (FEL) by electron microbunches in an undulator. An optical-FEL (OFEL) utilizes a counter-propagating laser pulse instead of an undulator, and has been proposed as a more compact and tunable source than a FEL. Yet, an OFEL is difficult to realize because of the high electron density required and subsequent high emittance. We demonstrate that broadband coherent XUV light, which in the temporal domain corresponds to a train of attosecond pulses with 8-as duration at 92-as intervals, can be generated by microbunching of relativistic electrons and positrons in an optical laser pulse. The symmetry between electrons and positrons in the bunch stabilizes the system and enables the rapid formation of dense microbunches over a ten-micrometer distance instead of the tens of meters typically required in an undulator. The high microbunch density and the stable spectral phase up to emitted photon energies of about 350 eV, allow for the creation of orders of magnitude more compact sources of XUV light that could be employed in physics, chemistry, biology, and industry.

## Introduction

Coherent pulses of soft x-rays are capable of tracking electron dynamics within atoms and molecules, which take place on attosecond time scales, and have a wide range of applications from materials characterization at near-atomic distances to the study of metabolic processes within cells [1, 2]. Yet, few compact laser-plasma sources of x-rays [3, 4] can rival the brightness of a free electron laser (FEL) [5]. A FEL produces coherent radiation via microbunching, induced by a seed (laser) [6, 7] or by the self-interaction of electrons with their radiation, known as self-amplified spontaneous emission (SASE) [8]. The microbunch separation occurs at the first harmonic  $\lambda_{\text{FEL}} = \lambda_u(1 + \frac{1}{2}K^2)/2\gamma_0^2$  emitted by ultra-relativistic (Lorentz factor  $\gamma_0 \gg 1$ ) electrons as they pass through an undulator of amplitude  $K = |e|B_0\lambda_u/2\pi m$ , magnetic field  $B_0$ , and spatial period  $\lambda_u$  [9]. Here, natural units  $c = \hbar = 4\pi\epsilon_0 = 1$  are employed, and we denote the particle's charge  $e$  and mass  $m$ , where  $e = -|e|$  for an electron.

The physical footprint of a FEL can be reduced dramatically by substituting a linear accelerator (linac) and undulator with a plasma-based accelerator [10, 11]. Here, electrons perform betatron oscillations of amplitude  $r_\beta$  around an ion column. Betatron radiation at the first harmonic  $\lambda_{\text{ICL}} = \lambda_\beta(1 + \frac{1}{2}a_\beta^2)/2\gamma_0^2$  is controlled by the amplitude  $a_\beta = 2\pi\gamma_0 r_\beta/\lambda_\beta$ , and can directly induce microbunching to create an ion channel laser (ICL) without an undulator [12–15]. The betatron wavelength  $\lambda_\beta = \sqrt{2\gamma_0}\lambda_{pl}$  depends on the plasma wavelength  $\lambda_{pl} = 2\pi\sqrt{m/4\pi n_- e^2}$  of a cold plasma with ambient electron density  $n_-$ . Although an ICL is compact,  $r_\beta$  and

hence  $a_\beta$  depend on the particle in question which makes an ICL difficult to realize [16], unlike a FEL, where  $K$  has the same value for all particles.

A compact optical-FEL (OFEL) could be created by replacing the undulator with a counter-propagating laser pulse of amplitude  $a_0 = |e|E_0/m\omega_0$ , peak electric field  $E_0$  and central frequency  $\omega_0 = 2\pi/\lambda_0$  [17–19]. In the case of an intense ( $a_0^2 \gg 1$ ), linearly polarized laser pulse, modelled as a plane wave, a quasi-continuous series of harmonics will be emitted on-axis starting from [20, 21]

$$\lambda_1 = \frac{\lambda_0}{4\gamma_0^2} \left(1 + \frac{1}{2}a_0^2\right). \quad (1)$$

Note that  $\lambda_1$  differs from  $\lambda_{\text{FEL}}$  by one-half, as the Lorentz-boost factors of  $\lambda_0$  and  $\lambda_u$  differ. In a plane wave  $a_0$  has the same value for all particles, like  $K$  and unlike  $a_\beta$ . Yet, current commercial lasers can access a range of amplitudes  $a_0 = 1\text{--}10$  [22] by changing the focal spot size, unlike an undulator where  $K$  is fixed by the magnet spacing and strength. This provides another degree of freedom in addition to  $\gamma_0$  for controlling the radiation properties. Therefore, an OFEL promises to be more compact and tunable than a typical FEL, yet is not acutely sensitive to the individual trajectories as in an ICL. However, OFELs use electron bunches which are required to have high densities due to the short duration of the laser field, thus facing the problems of Coulomb expansion and increase of emittance, which in turn hinders microbunch formation and coherent emission.

Here we demonstrate how broadband coherent XUV light can be obtained by microbunching of electrons and positrons ( $e^-/e^+$ ) in an intense laser pulse, operating at optical and UV wavelengths [see Fig. 1 for a schematic]. Radiation emitted from this system takes the form of an attosecond pulse train, with a well controlled spectral phase. The stability and neutrality of the  $e^-/e^+$  bunch suppresses Coulomb expansion and provides a restoring

\* michael.quin@mpi-hd.mpg.de

† a.dipiazza@rochester.edu

‡ matteo.tamburini@mpi-hd.mpg.de

force, which allows for sustained coherent emission and the rapid formation of microbunches. By considering an intense laser ( $a_0 = 5$ ) with wavelength 400 nm, we can utilize MeV-energy particles, readily obtained from a commercial, tabletop, linear accelerator or a compact plasma-based accelerator. Therefore, we show how an ultra-compact OFEL can be realized if a high quality, neutral particle beam is provided.

## Results

**Requirements of an  $e^-/e^+$  bunch.** To rapidly induce microbunching and then reduce the computational cost of the simulation, we consider a system of particles designed to emit coherently at the first harmonic. A bunch of  $N$  particles with initial density  $n_0$  tends to radiate coherently at  $\lambda_1$  providing the average interparticle distance satisfies  $R \sim 1/n_0^{1/3} \lesssim \lambda_1$  [23–25]. Therefore, coherent emission at a small wavelength necessarily requires a dense, high quality particle beam: for example, a relativistic  $\gamma_0 = 10$  bunch containing  $N = 10^3$  particles, colliding with a laser pulse of wavelength  $\lambda_0 = 1 \mu\text{m}$  and amplitude  $a_0 = 1$ , requires a density  $n_0 \gtrsim N/(4\pi\lambda_1^3/3) \sim 10^{21}$  particles/cm<sup>3</sup>. At these parameters an  $e^-$  beam would rapidly expand, which prevents coherent emission and microbunching, but a neutral bunch of  $e^-/e^+$  would remain stable, provided annihilation is unlikely. Remarkably, by considering an  $e^-/e^+$  bunch instead of an  $e^-/\text{ion}$  system, the equality of the  $e^-$  and  $e^+$  mass permits sustained synchronous oscillations, which greatly stabilize the system and improve the radiation yield.

High quality  $e^-$  beams with RMS kinetic energy spread  $\sigma_{\text{KE}} < 1\%$  and divergence  $\sigma_\theta < 1$  mrad are routinely produced by linacs. A relativistic  $e^-/e^+$  beam can then be created via the Bethe-Heitler process as charged particles propagate through a high- $Z$  target [26–29], which can be compressed to a bunch in a magnetic-chicane. A model demonstrating that resonance and microbunching occur at the harmonics of light emitted in a plane wave can be found in the Methods section. The microbunching process itself can assist in reaching relatively high densities [Fig. 1]. To demonstrate this robustly, we have proceeded from first principles by simulating *point* particles.

**Dynamics of point particles.** The solution of Maxwell’s equations for a point-like source are known as the (retarded) Liénard-Wiechert fields, which can be separated into ‘velocity’ and ‘acceleration’ parts, representing the Coulomb interaction and radiation respec-

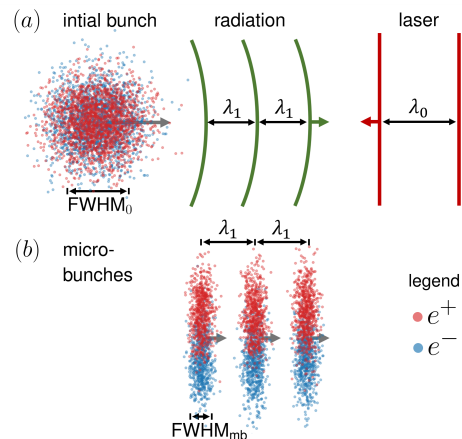


FIG. 1. **Schematic of microbunching in a laser pulse.** (a) Collision of  $e^-/e^+$  bunch with a plane wave of wavelength  $\lambda_0$  to produce harmonics of radiation starting from  $\lambda_1$ . (b) Microbunching due to the interaction of the bunch with its self-generated radiation, at the laser pulse peak. Here  $\lambda_1$  controls the microbunch separation and provides an upper limit of the width  $\text{FWHM}_{\text{mb}}$ . As drawn, (b) refers to the simulation results in Fig. 4 (d).

tively [30]

$$F_{\text{ret } i}^{\mu\nu}(x) = F_{\text{vel } i}^{\mu\nu}(x) + F_{\text{acc } i}^{\mu\nu}(x), \quad (2)$$

$$F_{\text{vel } i}^{\mu\nu}(x) = \left[ \frac{2e_i}{R_i^2} \frac{n_i^{[\mu} u_i^{\nu]}}{(n_i u_i)^3} \right]_{t_{\text{ret } i}}, \quad (3)$$

$$F_{\text{acc } i}^{\mu\nu}(x) = \left[ \frac{2e_i}{R_i} \frac{n_i^{[\mu} a_i^{\nu]}}{(n_i u_i)^2} - \frac{2e_i}{R_i} \frac{n_i^{[\mu} u_i^{\nu]}}{(n_i u_i)^3} (n_i a_i) \right]_{t_{\text{ret } i}}. \quad (4)$$

These describe the field seen at  $x^\mu = (t, \mathbf{x})$  and produced by the particle  $i$  with four-velocity  $u_i^\mu$  and four-acceleration  $a_i^\mu$ , separated by distance  $R_i = |\mathbf{x} - \mathbf{x}_i|$  in direction  $n_i^\mu = (x^\mu - x_i^\mu)/R_i$  at the retarded time  $t_{\text{ret } i} = t - R_i$ . Here we use the Minkowski metric  $\text{diag}(+1, -1, -1, -1)$  and short-hand notation  $(ab) \equiv a^\mu b_\mu$  and  $a^{[\mu} b^{\nu]} \equiv \frac{1}{2}(a^\mu b^\nu - a^\nu b^\mu)$ . If the observer is another distinct particle  $j \neq i$  then we refer to  $F_{\text{ret } i}^{\mu\nu}(x_j)$  as an ‘interparticle’ field, and if both particles are of the same species, as an ‘intraspecies’ field. For an  $e^-/e^+$  bunch, the classical description employed here is valid provided that in the common average rest-frame: (i) the average interparticle distance is well above the Bohr radius of positronium, to prevent bound state formation and annihilation, and (ii) the field experienced by each particle is much smaller than the critical field of quantum electrodynamics (QED)  $E_{\text{cr}} = m^2/|e| \approx 1.3 \times 10^{18}$  V/m, i.e. that  $\chi_0 \approx 2\gamma_0 E_0/E_{\text{cr}} \ll 1$  [31–33]. We ensured that both these conditions are well met throughout all our numerical simulations.

The total field acting on the  $i$ th particle  $\mathcal{F}_i^{\mu\nu} \equiv F_i^{\mu\nu}(x_i)$ , excluding the divergent self-field, is given by

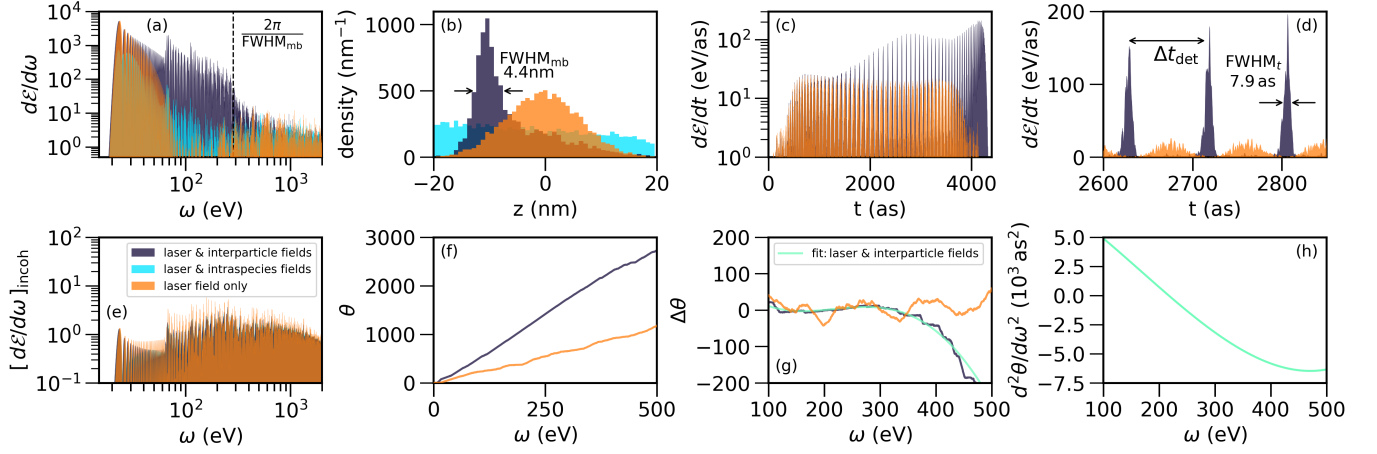


FIG. 2. **Collision of  $e^-/e^+$  bunch with  $\lambda_0 = 400$  nm laser.** (a) Spectrum of energy radiated onto  $1 \text{ cm}^2$  detector at  $1 \text{ m}$  distance along  $+z$  from the bunch-laser pulse collision region, with first harmonic  $\omega_1 \approx 23 \text{ eV}$ . (b) Bunch compression at laser pulse peak. (c) Attosecond pulse train observed at detector. (d) Properties of attosecond pulses; time interval  $\Delta t_{\text{det}} \approx 92 \text{ as}$ . (e) Spectrum of incoherent energy radiated onto detector; field configurations are overlapping and indistinguishable. (f) Spectral phase of radiation. (g) Residual spectral phase. (h) Group delay dispersion evaluated from the polynomial fit in (g). Legends in (e) and (g) apply to all plots.

the external laser field and the interparticle fields

$$\mathcal{F}_i^{\mu\nu}(x_i) = F_{\text{ext}}^{\mu\nu}(x_i) + \sum_{\substack{j=1 \\ j \neq i}}^N F_{\text{ret } j}^{\mu\nu}(x_i). \quad (5)$$

The particles' trajectories can be evaluated by integrating the reduced Landau-Lifshitz (LL) equation [34, 35]

$$m_i a_i^\mu = e_i \mathcal{F}_i^{\mu\nu} u_{\nu,i} + \frac{2e_i^4}{3m_i^2} \left[ \mathcal{F}_i^{\mu\nu} \mathcal{F}_{\nu\alpha,i} u_i^\alpha + (\mathcal{F}_i u_i)^2 u_i^\mu \right], \quad (6)$$

which accounts for the energy and momentum loss during the emission of radiation via the self-force, an effect known as radiation reaction (RR) [30, 31]. Here 'reduced' indicates that we have neglected a term containing the first derivatives of the fields as it induces effects typically far smaller than quantum-mechanical corrections [36]. The self-force is parameterized by  $R_C = \alpha \chi_0 a_0$ , where  $\alpha \approx 1/137$  is the fine structure constant [31]. In our simulations, RR will play a minor role ( $R_C \ll 1$ ) with little impact on the microbunching observed, nevertheless we include this effect to ensure self-consistency. With the trajectories known, the spectrum of energy radiated per unit solid angle  $\Omega$  as seen by a distant observer in direction  $n^\mu = (1, \mathbf{n})$ , satisfying  $(n)^\mu (n)_\mu = 0$ , is  $d\mathcal{E}/d\omega d\Omega = (4\pi^2)^{-1} |\sum_{i=1}^N \mathcal{I}_i(\omega, \mathbf{n})|^2$ , where the radiation integral is defined as [37]

$$\mathcal{I}_i(\omega, \mathbf{n}) = e_i \int_{-\infty}^{+\infty} \frac{d}{dt} \left[ \frac{\mathbf{n} \times (\mathbf{n} \times \mathbf{u}_i)}{(n u_i)} \right] e^{i\omega(n x_i)} dt. \quad (7)$$

The incoherent part of the spectrum is similarly defined as  $[d\mathcal{E}/d\omega d\Omega]_{\text{incoh}} = (4\pi^2)^{-1} \sum_{i=1}^N |\mathcal{I}_i(\omega, \mathbf{n})|^2$ .

Details of the numerical code [24, 34] developed to solve this system of equations can be found in the Methods section. A key advantage over alternative codes is the

separation of interparticle fields into acceleration and velocity components. By 'switching off' the velocity fields  $F_{\text{vel } j}^{\mu\nu}(x_i) = 0$  from all particles  $j$ , we can isolate the role of the radiation, which induces microbunching, from the electrostatic attraction between  $e^-$  and  $e^+$ , which stabilizes the bunch and maintains coherence (see Fig. 3 and the discussion below).

**Simulation setup.** Two particles separated by a distance  $R$  with identical initial velocity tend to radiate coherently at frequency  $\omega$  when  $\omega R < \pi$  [23, 25]. Analogously, a bunch of width  $\text{FWHM}_0$  is expected to emit coherent radiation for  $\omega \text{FWHM}_0 \lesssim 2\pi$ , as confirmed by Fig. 2. In all simulations, we consider a neutral Gaussian  $e^-/e^+$  bunch of  $\text{FWHM}_0 = 16 \text{ nm}$  containing  $4000 e^-$  and  $4000 e^+$ , moving along  $+z$  with  $2.0 \text{ MeV}$  kinetic energy ( $\gamma_0 = 5$ ),  $\sigma_{\text{KE}} = 0.1\%$  kinetic energy spread, and  $\sigma_\theta = 1 \text{ mrad}$  divergence. One can show the average interparticle distance in the rest frame  $R \approx 24 a_{\text{ps}}$  is an order of magnitude above the Bohr radius for positronium  $a_{\text{ps}} \approx 0.11 \text{ nm}$ , indicating that bound state formation and  $e^-/e^+$  annihilation are unlikely [24]. This remains true throughout the simulation.

The  $e^-/e^+$  bunch collides head-on with a laser pulse, linearly polarized along  $x$  and propagating along  $-z$ , which we model as a plane wave pulse. In the Methods section, we show that the plane wave approximation has no significant impact on our simulation results, and allows the microbunching effect to be demonstrated with a simple analytical model. The laser pulse has a fixed amplitude  $a_0 = 5$  and pulse length  $\text{FWHM}_L \approx 26.7 \text{ fs}$ , while the wavelength varies  $\lambda_0 = [400, 200, 100] \text{ nm}$  depending on the simulation in question, as does the cycle-averaged peak intensity  $I_0 \approx [2.2, 8.7, 35] \times 10^{20} \text{ W/cm}^2$ , for each wavelength respectively. Such parameters can

be obtained with commercially available systems. For example, the second harmonic of a Ti:Sa laser (400 nm) can be produced with efficiencies well above 50% [38]. A small time step  $\Delta t \approx 0.27$  as was used to carefully resolve the interparticle fields and high frequency radiation. Note that the self-force, i.e., RR plays a minor role  $R_C \approx [1.1, 2.2, 4.4] \times 10^{-5}$ , and QED corrections are negligible  $\chi_0 \approx [3.0, 6.0, 12.1] \times 10^{-4}$  in our simulations.

In order to unveil the physics of microbunching, we consider several configurations for the field  $\mathcal{F}_i^{\mu\nu}(x_i)$  when solving the reduced LL equation: (i) ‘laser & interparticle fields’, where particles interact with the total field in Eq. (5), (ii) ‘laser & intraspecies fields’, where particles interact with the total field *excluding* fields from *different species* of particles, that is the  $e^-$  and  $e^+$  do not interact, and (iii) ‘laser field only’, where particles interact with only the external laser field. In addition, we consider (iv) ‘laser & acceleration fields’, which is the same as (i) except the velocity fields have been switched off in the simulation.

**Bunch compression via radiation emission.** Figure 2 shows the simulation results of the  $e^-/e^+$  bunch colliding with the  $\lambda_0 = 400$  nm laser pulse for each field configuration. Note that frequency-doubled lasers operating at  $\lambda_0 = 400$  nm are widely available [39, 40]. By comparing the total [Fig. 2 (a)] and incoherent [Fig. 2 (e)] spectra, frequencies at which coherent emission occurs can be identified, and then explained by examining the bunch dynamics at the laser pulse peak [Fig. 2 (b)]. The spectrum is characterized by a broad series of harmonics beginning at  $\omega_1 \approx 23$  eV or  $\lambda_1 \approx 55$  nm, at which coherent emission always occurs due to the small size of the initial bunch. For ‘laser field only’, the bunch width remains stable at  $\text{FWHM}_0$  throughout the simulation, and one can see coherence for  $\omega \lesssim 2\pi/\text{FWHM}_0 \approx 78$  eV. For ‘laser & interparticle fields’, the bunch is compressed by the emitted radiation to  $\text{FWHM}_{\text{mb}}$  approximately one-quarter of its initial width, which leads to increased coherence at correspondingly high frequencies  $\omega \lesssim 2\pi/\text{FWHM}_{\text{mb}} \approx 280$  eV [see Fig. 2 (a)].

**Attosecond pulse train.** In Fig. 2 (f), the spectral phase  $\theta \equiv \theta(\omega)$  of the transversely polarized radiation emitted in forward direction is shown, defined by  $\rho(\omega)e^{i\theta(\omega)} \equiv \sum_{i=1}^N \mathcal{I}_i(\omega, \hat{\mathbf{z}}) \cdot \hat{\mathbf{x}}$ . Notice that  $\theta$  increases linearly, and is particularly well behaved when interparticle fields are included. A spectral phase which varies linearly with frequency corresponds to a temporal shift of the time-dependent signal. Therefore, a linear fit has been subtracted from Fig. 2 (f) to obtain the residual phase  $\Delta\theta$  in Fig. 2 (g). For ‘laser & interparticle fields’, one notices the residual phase is relatively flat up to  $\sim 350$  eV. To estimate the group delay dispersion, we have plotted the second derivative of the polynomial fit of the residual phase in Fig. 2 (h), where it remains in the order of  $-3000$  as<sup>2</sup> at 300 eV. The attosecond pulse train is plotted in Fig. 2 (c) and one can see the temporal prop-

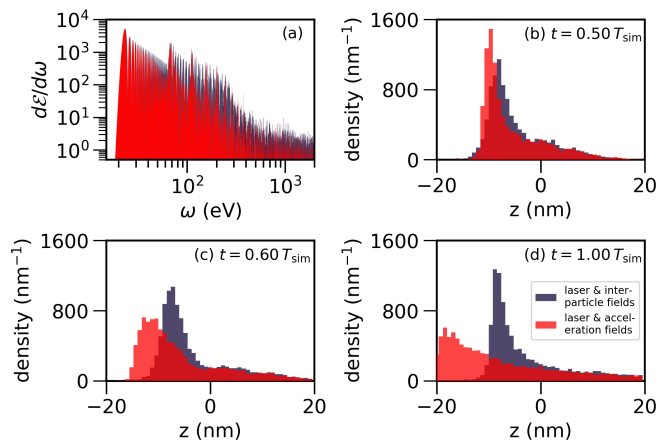


FIG. 3. **Collision of  $e^-/e^+$  bunch with  $\lambda_0 = 400$  nm laser, with and without velocity fields.** (a) Spectrum radiated onto detector. (b) Bunch at laser pulse peak. (c) Bunch at intermediate time. (d) Bunch at end of simulation. Legend in (d) applies to all plots,  $T_{\text{sim}}$  is the simulation duration.

erties of the pulses in Fig. 2 (d), where the time interval between pulses  $\Delta t_{\text{det}} \approx 92$  as agrees with our model (see Methods section).

**Microbunch formation and the role of the positrons.** In Fig. 2, the interaction of the  $e^-/e^+$  bunch with its emitted radiation led to bunch compression and increased coherence. In order to further clarify the physical mechanism of microbunching we have repeated this simulation without velocity fields in Fig. 3. By switching off the velocity fields, we reduce the energy radiated onto the detector by approximately one-third [Fig. 3 (a)]. To explain this, consider the longitudinal distribution of particles throughout the simulation. At the laser pulse peak [Fig. 3 (b)] the bunch is compressed regardless of whether the velocity fields are included. This confirms that the acceleration fields (radiation) compress the bunch. At advanced times [Fig. 3 (c,d)], the bunch remains stable and localized only when velocity fields are included, which suggests that they provide a restoring force which allows for sustained coherent emission over a longer time period.

Moreover, to highlight the role of the positrons, we observe that all simulations with ‘laser & intraspecies fields’, where the  $e^-$  and  $e^+$  artificially do not feel each other’s fields, suffer from a Coulomb explosion which prevents bunch compression and hinders coherent emission [see the light blue line in Fig. 2 (a,b)]. This underlines the need for a neutral particle beam to create a functioning OFEL.

**Generation of multiple microbunches.** A long particle beam  $\text{FWHM}_0 \gg \lambda_1$  with a similar density as our initial bunch would be required to observe multiple microbunches. A simulation from first principles is unfeasible in this scenario given the computational resources required (see Methods section). Instead, as a proof of prin-



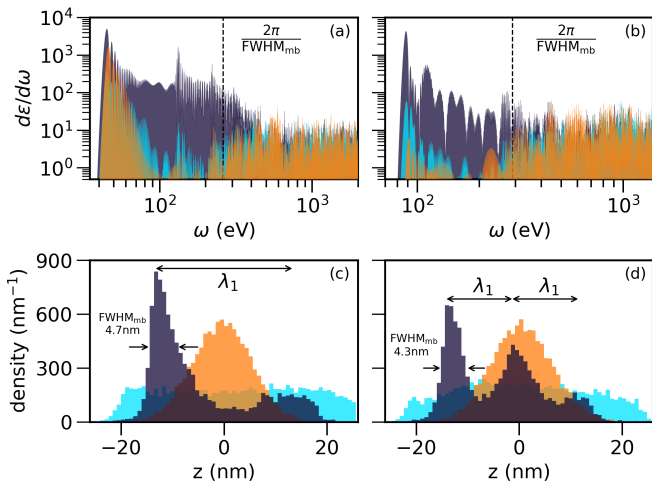


FIG. 4. **Microbunching of  $e^-/e^+$  in lasers of various wavelengths.** (a) Spectrum radiated onto detector and (c) microbunching at pulse peak for  $\lambda_0 = 200$  nm. (b) Spectrum radiated onto detector and (d) microbunching at pulse peak for  $\lambda_0 = 100$  nm. Microbunch separation occurs at (c)  $\lambda_1 \approx 28$  nm and (d)  $\lambda_1 \approx 14$  nm. Legend in Fig. 2 (e) applies here.

principle, we can leave the bunch unchanged and increase the laser frequency, therefore reducing  $\lambda_1$ . Consider then, a collision between the  $e^-/e^+$  bunch with lasers of various wavelengths: in Fig. 4 (c) and (d) we can see two and three microbunches respectively, for  $\lambda_0 = 200$  nm and  $\lambda_0 = 100$  nm. Note that the microbunch separation occurs consistently at the first harmonic  $\lambda_1$ . For both wavelengths, the width of the dominant microbunch is approximately one-quarter of the initial bunch, increasing the coherence of the emitted radiation [Fig. 4 (a, b)]. Finally, we note that the microbunching observed in Fig. 4 (d) was successfully reproduced with the PIC codes OSIRIS [41] and SMILEI [42].

## Discussion

As the initial bunch is small compared to the plasma skin depth  $\delta_p = 1/\omega_p \approx 94$  nm, this implies plasma instabilities do not affect the dynamics. Here the plasma frequency is  $\omega_p = \sqrt{8\pi n_0 e^2/m_0}$ , which includes an extra factor  $\sqrt{2}$  with respect to an electron-ion plasma to account for the equal mass of  $e^-$  and  $e^+$  [29]. In our simulations, the trajectories are dominated by the laser with transverse oscillations of amplitude  $r = a_0/2\gamma_0\omega_0$ , where  $r \approx [32, 16, 8]$  nm for each wavelength  $\lambda_0 = [400, 200, 100]$  nm respectively, as opposed to an ICL where the amplitude of the oscillations depend on the initial conditions of the particle.

A typical seeded FEL produces narrow-band pulses of  $\sim 10$  fs duration at  $\lambda_{\text{FEL}} \sim 10$  nm from ultra-relativistic electrons  $\gamma_0 \approx 10^3$  [43]. Here we have observed a broad spectrum of coherent XUV light starting from the first harmonic  $\lambda_1$ , which is of the same order of magnitude as  $\lambda_{\text{FEL}}$ . However, we require only mildly relativistic particles with  $\gamma_0 = 5$ , which can be produced from a commer-

cial tabletop linac or a compact plasma-based accelerator. While the magnet-spacing  $\lambda_u$  and hence undulator amplitude  $K$  are difficult to change in a FEL,  $a_0$  can easily be varied via the focal spot size allowing the spectral properties to be changed as desired. In the scheme proposed here, radiation is emitted in pulses of duration  $\sim 8$  as at low intensity due to the small number of particles that can be simulated ( $N = 8000$ ) with our computational resources. Note, however, that the yield for coherent emission scales quadratically with the number of particles emitting coherently. In comparison, recent experiments have observed pulses of duration  $\sim 100$  as from a FEL [44] with a macroscopically large number of electrons. Further work will be required to generalize the mechanism studied here to a macroscopically large  $e^-/e^+$  beam. However, in Fig. 4, we have already demonstrated that the formation of a microbunch train is feasible. In addition, note that the residual phase is flat for  $\omega \lesssim 350$  eV in Fig. 2 (g), within the water window range of frequencies (280 to 530 eV), of particular importance for observing biological processes over attosecond time scales [45–48].

In summary, we have demonstrated how pulses of broadband, coherent XUV light can be produced from the collision of an  $e^-/e^+$  bunch with a laser pulse. Coherent emission takes place due to microbunch formation via SASE on a length scale of  $\text{FWHM}_L \sim 10$   $\mu\text{m}$ , six orders of magnitude smaller than the length of a typical undulator  $\sim 10$  m, potentially allowing for an ultra-compact light source. The spectral and temporal properties of the radiation are well controlled inside the water window. The challenge, as always for FELs, lies in creating a high quality particle beam to realize this scheme. For the particle densities considered here, we have demonstrated that microbunching with electrons alone is virtually impossible due to Coulomb repulsion; a neutral beam will be necessary if one wishes to see microbunching over microscopic distances. These results constitute a proof of principle of a new tabletop source of temporally coherent broadband XUV radiation, with broad applications in physics, chemistry, and biology as well as in industry.

## Methods

**Numerical code.** Equations (2)–(7) are solved numerically as follows: our code is initialized by assuming the particles propagate ballistically before colliding with the laser pulse (a sensible assumption for a neutral bunch). The trajectories are stored at discrete time steps in the memory, and the fields in Eqs. (2)–(4) are evaluated at the retarded time(s) by interpolation. Then, the reduced LL equation (6) is integrated with a second-order leapfrog scheme [36]. Finally, the radiation spectrum (7) is found via a fast Fourier transform. This approach allows a simple system to be studied in detail from first principles. However, the number of particles  $N$  and the spatial extent that can be simulated is limited by the need to keep the entire trajectories of all particles in the memory. The

computational cost  $O(N^2)$  increases rapidly with  $N$ , and hence we are limited to  $N \lesssim 10^4$  given the computational resources available. Further information and tests of the code can be found in Ref. [24].

### Approximating the laser as a plane wave pulse.

In our simulations, we consider a laser pulse modeled as a plane wave pulse with vector potential

$$\frac{|e|}{m} \mathbf{A}_{\text{ext}}(\varphi) = a(\varphi) \sin(\varphi) \hat{\mathbf{x}}, \quad (8)$$

$$a(\varphi) = a_0 \cos^2(\varphi/\Delta). \quad (9)$$

The four-potential  $A_{\text{ext}}^\mu(\varphi) = (0, \mathbf{A}_{\text{ext}}(\varphi))$  is chosen to satisfy the Lorenz gauge ( $\partial A_{\text{ext}}(\varphi) = 0$ ). The pulse propagates along  $-z$  with wave phase  $\varphi = \omega_0 z_+$ , where  $z_\pm = t \pm z$  are the light-cone coordinates. The envelope satisfies  $a(\varphi_0) = 0$  at the initial phase  $\varphi_0 = -\pi\Delta/2$ , and the envelope domain is  $\varphi \in [-\pi\Delta/2, +\pi\Delta/2]$ .

In the regime of interest here, where  $a_0 \approx \gamma_0$ , the plane wave approximation is valid when the laser waist is much larger than the transverse bunch width (initially 16 nm). Another simulation has been carried out considering a focused laser with linear polarization,  $\lambda_0 = 400$  nm,  $a_0 = 5$  and a waist radius  $w_0 = 4$   $\mu\text{m}$ ; this leaves the results as plotted in Fig. 2 unchanged. For the focused laser field employed see Ref. [49], where we have considered terms up to third order in the diffraction angle.

**Trajectory in a plane wave.** Consider a particle colliding head-on with the external plane wave pulse. Neglecting radiation reaction, the four-velocity can be written in terms of the light-cone coordinates  $u_\pm \equiv \gamma \pm u_z$  [31, 35]

$$\mathbf{u}_\perp(\varphi) = -\frac{e}{m} \mathbf{A}_{\text{ext}}(\varphi), \quad (10)$$

$$u_-(\varphi) = \frac{1}{u_{0,+}} [1 + \mathbf{u}_\perp^2(\varphi)], \quad (11)$$

$$u_+(\varphi) = u_{0,+}. \quad (12)$$

In our simulations, when the trajectory differs from Eqs. (10)–(12), this indicates the cumulative effect of interparticle fields or RR become important.

**Model of microbunching.** Here we demonstrate that resonance, energy transfer and microbunching can occur at the harmonics of reflected light in a plane wave. The method employed is similar to explanations of microbunching in a low gain FEL [9]. Since the aim is to show at which frequencies most of the energy is transferred from the electrons to the radiation, we start our considerations from the evolution of the Lorentz factor for a single particle

$$\frac{d\gamma}{d\varphi} = \frac{e\mathbf{E}(\varphi) \cdot \mathbf{u}(\varphi)}{m\omega_0 u_{0,+}}, \quad (13)$$

where we have used  $d\varphi/d\tau = \omega_0 u_{0,+}$  with  $\tau$  being the proper time. As the  $e^-/e^+$  bunch is quasi-neutral

throughout the simulation we neglect Coulomb fields here. Then, the total field depends on the external laser field and a radiation field  $\mathbf{E}(\varphi) = \mathbf{E}_{\text{ext}}(\varphi) + \mathbf{E}_{\text{rad}}(\varphi)$ . We assume the radiation field can be approximated as an arbitrary series of plane waves propagating along  $+z$  with transverse polarization

$$\mathbf{E}_{\text{rad}}(\varphi) = \sum_l \mathbf{E}_{l,\perp} \sin \phi_l(\varphi), \quad (14)$$

where  $\phi_l(\varphi) = \omega_l z_-(\varphi) + \psi_l$  is the radiation wave phase,  $\omega_l$  is the frequency, and  $\psi_l$  is an arbitrary constant phase. In the monochromatic approximation  $\Delta \gg 1$  we have  $a(\varphi) \approx a_0$ . For example, in our simulation for  $\lambda_0 = 400$  nm we have  $\Delta \approx 110$ . One can then derive an expression for the position  $z_-(\varphi) = z_{0,-} + \int_{\varphi_0}^{\varphi} [u_-(\varphi')/(\omega_0 u_{0,+})] d\varphi'$ , to obtain

$$z_-(\varphi) - z_{0,-} = \frac{1}{\omega_0 u_{0,+}^2} \left[ \left(1 + \frac{a_0^2}{2}\right) (\varphi - \varphi_0) - \frac{a_0^2}{4} [\sin(2\varphi) - \sin(2\varphi_0)] \right]. \quad (15)$$

By comparing the particles' trajectories in our simulations to the exact solutions in a plane wave [Eqs. (10)–(12)], we know that the external field dominates the system  $|\mathbf{E}_{\text{rad}}(\varphi)| \ll |\mathbf{E}_{\text{ext}}(\varphi)|$ , and therefore the effect of the radiation field on the trajectory can be treated perturbatively. Under the assumption that the particles trajectory is determined by the plane wave, on average, there is no energy exchanged between the particle and external plane-wave field  $\langle \mathbf{E}_{\text{ext}}(\varphi) \cdot \mathbf{u}_\perp \rangle = 0$ , where the cycle-average is defined as  $\langle f(\varphi) \rangle = \frac{1}{2\pi} \int_{\varphi-\pi}^{\varphi+\pi} f(\varphi') d\varphi'$  for a generic function of the phase  $f(\varphi)$ . The average energy exchanged between the particle and radiation field is then

$$\left\langle \frac{d\gamma}{d\varphi} \right\rangle = \sum_l \frac{a_0 |e| E_{l,x}}{2m\omega_0 u_{0,+}} \text{Re} \left[ \langle e^{i\eta_+^l(\varphi)} \rangle - \langle e^{i\eta_-^l(\varphi)} \rangle \right], \quad (16)$$

where  $\eta_\pm^l(\varphi) = \phi_l(\varphi) \pm \varphi$  and  $E_{l,x} = \mathbf{E}_{l,\perp} \cdot \hat{\mathbf{x}}$ . One can solve these integrals using Bessel functions

$$\text{Re} \langle e^{i\eta_\pm^l(\varphi)} \rangle = \sum_{n=-\infty}^{\infty} J_n(\rho_l) \frac{\sin(\pi\Theta_{l,n}^\pm)}{\pi\Theta_{l,n}^\pm} \cos(\Theta_\pm^{l,n} \varphi + \psi_l'), \quad (17)$$

where  $\rho_l = \omega_l a_0^2 / 4\omega_0 u_{0,+}^2$ , and we have used the generating function [50]

$$e^{-i\rho_l \sin(2\varphi)} = \sum_{n=-\infty}^{\infty} J_n(\rho_l) e^{-2in\varphi}. \quad (18)$$

Note that the coefficient of  $\varphi$  in the phase of each harmonic is given by

$$\Theta_\pm^{l,n} = \frac{\omega_l}{u_{0,+}^2 \omega_0} \left(1 + \frac{a_0^2}{2}\right) - 2n \pm 1, \quad (19)$$

and  $\psi'_l$  is the modified constant phase, defined as

$$\psi'_l = \psi_l + \omega_l z_{0,-} - \frac{\omega_l}{\omega_0 u_{0,+}^2} \left[ \left( 1 + \frac{a_0^2}{2} \right) \varphi_0 - \frac{a_0^2 \sin(2\varphi_0)}{4} \right]. \quad (20)$$

For each frequency  $\omega_l$ , the dominant contribution from the sum over  $n$  occurs at  $\Theta_{\pm}^{l,n} = 0$ . If averaged over an infinite number of cycles instead of a single cycle as above, a delta function would collapse the sum over  $n$  leaving only terms where  $n = l$ . We conclude that resonance occurs at  $\Theta_{\pm}^{l,n} = 0$ , such that (taking  $n = l$ )

$$\frac{\omega_l}{4\gamma_0^2 \omega_0} = \frac{2l - 1}{1 + \frac{1}{2}a_0^2}, \quad (21)$$

for a relativistic particle  $u_{0,+}^2 \approx 4\gamma_0^2$ . These are exactly the harmonics emitted in a monochromatic plane wave [20, 21]. In practice,  $\lambda_1 = 2\pi/\omega_1$  is the longest emitted harmonic, and emission at this wavelength scales coherently with  $N^2$  such that it dominates the system and any subsequent microbunching.

We note a limitation of this model: our assumption that  $\mathbf{E}_{l,\perp}$  is constant. From our simulations in Fig. 2(c) with ‘laser & interparticle fields’, the amplitude of the radiation field actually increases over time, as opposed to remaining constant. Therefore, this model cannot predict the intensity of radiation emitted quantitatively, but does suffice to predict the resonant wavelength at which microbunching occurs.

**Time interval between radiation pulses.** The light-cone coordinate  $z_-(\varphi)$  in Eq. (15) can be interpreted as the time measured by the detector. For one oscillation of the plane wave, the particle’s radiation cone will sweep across the detector twice. Therefore, the time period between radiation pulses is the change in  $z_-(\varphi)$  over half a cycle

$$\Delta t_{\text{det}} = z_-(\varphi + \pi) - z_-(\varphi) \approx \frac{T_0}{8\gamma_0^2} \left( 1 + \frac{a_0^2}{2} \right). \quad (22)$$

Here  $T_0 = 2\pi/\omega_0$  is the plane wave period and we have assumed the particle is relativistic. For example, with wavelength  $\lambda_0 = 400$  nm one can expect radiation pulses separated by a time interval  $\Delta t_{\text{det}} \approx 92$  as in excellent agreement with Fig. 2(d).

## Data availability

Data which supports the findings of this paper is available upon reasonable request to M.J.Q.

## Code availability

The working principles of our code have been outlined in this paper, and we have included references where one can find further details and tests of the code. In future, we aim to make this code available for public use; before then, it can be made available upon reasonable request to M.J.Q.

## References

- [1] M. F. Ciappina, J. A. Pérez-Hernández, A. S. Landsman, W. A. Okell, S. Zherebtsov, B. Förg, J. Schötz, L. Seifert, T. Fennel, T. Shaaran, T. Zimmermann, A. Chacón, R. Guichard, A. Zaïr, J. W. G. Tisch, J. P. Marangos, T. Witting, A. Braun, S. A. Maier, L. Roso, M. Krüger, P. Hommelhoff, M. F. Kling, F. Krausz, and M. Lewenstein, Attosecond physics at the nanoscale, *Rep. Prog. Phys.* **80**, 054401 (2017).
- [2] F. Krausz and M. Ivanov, Attosecond physics, *Rev. Mod. Phys.* **81**, 163 (2009).
- [3] M. Hentschel, R. Kienberger, C. Spielmann, G. A. Reider, N. Milosevic, T. Brabec, P. Corkum, U. Heinzmann, M. Drescher, and F. Krausz, Attosecond metrology, *Nature* **414**, 509 (2001).
- [4] J. W. Wang, M. Zepf, and S. G. Rykovanov, Intense attosecond pulses carrying orbital angular momentum using laser plasma interactions, *Nat. Commun.* **10**, 5554 (2019).
- [5] Z. Huang and K.-J. Kim, Review of x-ray free-electron laser theory, *Phys. Rev. ST Accel. Beams* **10**, 034801 (2007).
- [6] P. K. Maroju, C. Grazioli, M. Di Fraia, M. Muioli, D. Ertel, H. Ahmadi, O. Plekan, P. Finetti, E. Allaria, L. Giannessi, G. De Ninno, C. Spezzani, G. Penco, S. Spampinati, A. Demidovich, M. B. Danailov, R. Borghes, G. Kourousias, C. E. Sanches Dos Reis, F. Billé, A. A. Lutman, R. J. Squibb, R. Feifel, P. Carpeggiani, M. Rezzuzzi, T. Mazza, M. Meyer, S. Bengtsson, N. Ibrakovic, E. R. Simpson, J. Mauritsson, T. Csizmadia, M. Dumergue, S. Kühn, H. Nandiga Gopalakrishna, D. You, K. Ueda, M. Labeye, J. E. Bækhoj, K. J. Schafer, E. V. Gryzlova, A. N. Grum-Grzhimailo, K. C. Prince, C. Callegari, and G. Sansone, Attosecond pulse shaping using a seeded free-electron laser, *Nature* **578**, 386 (2020).
- [7] E. Allaria, R. Appio, L. Badano, W. A. Barletta, S. Bassanese, S. G. Biedron, A. Borga, E. Busetto, D. Castonovo, P. Cinquegrana, S. Cleva, D. Cocco, M. Cornacchia, P. Craievich, I. Cudin, G. D’Auria, M. Dal Forno, M. B. Danailov, R. De Monte, G. De Ninno, P. Delgiusto, A. Demidovich, S. Di Mitri, B. Diviacco, A. Fabris, R. Fabris, W. Fawley, M. Ferianis, E. Ferrari, S. Ferry, L. Froehlich, P. Furlan, G. Gaio, F. Gelmetti, L. Giannessi, M. Giannini, R. Gobessi, R. Ivanov, E. Karantzoulis, M. Lanza, A. Lutman, B. Mahieu, M. Milloch, S. V. Milton, M. Musardo, I. Nikolov, S. Noe, F. Parmigiani, G. Penco, M. Petronio, L. Pivetta, M. Predonzani, F. Rossi, L. Rumiz, A. Salom, C. Scafuri, C. Serpico, P. Sigalotti, S. Spampinati, C. Spezzani, M. Svandrlík, C. Svetina, S. Tazzari, M. Trovo, R. Umer, A. Vascotto, M. Veronese, R. Visintini, M. Zaccaria, D. Zangrando, and M. Zangrando, Highly coherent and stable pulses from the fermi seeded free-electron laser in the extreme ultraviolet, *Nat. Photonics* **6**, 699 (2012).
- [8] P. Emma, R. Akre, J. Arthur, R. Bionta, C. Bostedt, J. Bozek, A. Brachmann, P. Bucksbaum, R. Coffee, F.-J. Decker, Y. Ding, D. Dowell, S. Edstrom, A. Fisher, J. Frisch, S. Gilevich, J. Hastings, G. Hays, P. Hering, Z. Huang, R. Iverson, H. Loos, M. Messer-

- schmidt, A. Miahnahri, S. Moeller, H.-D. Nuhn, G. Pile, D. Ratner, J. Rzepiela, D. Schultz, T. Smith, P. Stefan, H. Tompkins, J. Turner, J. Welch, W. White, J. Wu, G. Yocky, and J. Galayda, First lasing and operation of an ångstrom-wavelength free-electron laser, *Nat. Photonics* **4**, 641 (2010).
- [9] P. Schmäser, M. Dohlus, J. Rossbach, and C. Behrens, *Ultraviolet and Soft X-Ray Free-Electron Lasers*, 2nd ed. (Springer Berlin Heidelberg, 2009).
- [10] M. Labat, J. C. Cabadağ, A. Ghaith, A. Irman, A. Berlioux, P. Berteaud, F. Blache, S. Bock, F. Bouvet, F. Briquez, Y.-Y. Chang, S. Corde, A. Debus, C. De Oliveira, J.-P. Duval, Y. Dietrich, M. El Ajjouri, C. Eisenmann, J. Gautier, R. Gebhardt, S. Grams, U. Helbig, C. Herbeaux, N. Hubert, C. Kitegi, O. Kononenko, M. Kuntzsch, M. LaBerge, S. Lê, B. Leluan, A. Loulergue, V. Malka, F. Marteau, M. H. N. Guyen, D. Oumbarek-Espinos, R. Pausch, D. Pereira, T. Püschel, J.-P. Ricaud, P. Rommeluere, E. Roussel, P. Rousseau, S. Schöbel, M. Sebdaoui, K. Steiniger, K. Tavakoli, C. Thauray, P. Ufer, M. Valléau, M. Vandenberghe, J. Vétéran, U. Schramm, and M.-E. Couprie, Seeded free-electron laser driven by a compact laser plasma accelerator, *Nat. Photonics* **17**, 150 (2023).
- [11] A. F. Habib, G. G. Manahan, P. Scherkl, T. Heinemann, A. Sutherland, R. Altuiri, B. M. Alotaibi, M. Litos, J. Cary, T. Raubenheimer, E. Hemsing, M. J. Hogan, J. B. Rosenzweig, P. H. Williams, B. W. J. McNeil, and B. Hidding, Attosecond-ångstrom free-electron-laser towards the cold beam limit, *Nat. Commun.* **14**, 1054 (2023).
- [12] E. Esarey, C. B. Schroeder, and W. P. Leemans, Physics of laser-driven plasma-based electron accelerators, *Rev. Mod. Phys.* **81**, 1229 (2009).
- [13] A. Rousse, K. T. Phuoc, R. Shah, A. Pukhov, E. Lefebvre, V. Malka, S. Kiselev, F. Burgy, J.-P. Rousseau, D. Umstadter, and D. Hulin, Production of a keV x-ray beam from synchrotron radiation in relativistic laser-plasma interaction, *Phys. Rev. Lett.* **93**, 135005 (2004).
- [14] S. Cipiccia, M. R. Islam, B. Ersfeld, R. P. Shanks, E. Brunetti, G. Vieux, X. Yang, R. C. Issac, S. M. Wiggins, G. H. Welsh, M.-P. Anania, D. Maneuski, R. Montgomery, G. Smith, M. Hoek, D. J. Hamilton, N. R. C. Lemos, D. Symes, P. P. Rajeev, V. O. Shea, J. M. Dias, and D. A. Jaroszynski, Gamma-rays from harmonically resonant betatron oscillations in a plasma wake, *Nat. Phys.* **7**, 867 (2011).
- [15] X. Davoine, F. Fiúza, R. A. Fonseca, W. B. Mori, and L. O. Silva, Ion-channel laser growth rate and beam quality requirements, *J. Plasma Phys.* **84**, 905840304 (2018).
- [16] E. Esarey, B. A. Shadwick, P. Catravas, and W. P. Leemans, Synchrotron radiation from electron beams in plasma-focusing channels, *Phys. Rev. E* **65**, 056505 (2002).
- [17] J. Gea-Banacloche, G. Moore, R. Schlicher, M. Scully, and H. Walth, Soft x-ray free-electron laser with a laser undulator, *IEEE J Quant Electr.* **23**, 1558 (1987).
- [18] J. Gallardo, R. Fernow, R. Palmer, and C. Pellegrini, Theory of a free-electron laser with a gaussian optical undulator, *IEEE J Quant Electr.* **24**, 1557 (1988).
- [19] K. Steiniger, D. Albach, M. Bussmann, M. Loeser, R. Pausch, F. Röser, U. Schramm, M. Siebold, and A. Debus, Building an optical free-electron laser in the traveling-wave thomson-scattering geometry, *Frontiers in Physics* **6** (2019).
- [20] E. S. Sarachik and G. T. Schappert, Classical theory of the scattering of intense laser radiation by free electrons, *Phys. Rev. D* **1**, 2738 (1970).
- [21] Y. I. Salamin and F. H. M. Faisal, Harmonic generation by superintense light scattering from relativistic electrons, *Phys. Rev. A* **54**, 4383 (1996).
- [22] C. N. Danson, C. Haefner, J. Bromage, T. Butcher, J.-C. F. Chanteloup, E. A. Chowdhury, A. Galvanauskas, L. A. Gizzi, J. Hein, D. I. Hillier, N. W. Hopps, Y. Kato, E. A. Khazanov, R. Kodama, G. Korn, R. Li, Y. Li, J. Limpert, J. Ma, C. H. Nam, D. Neely, D. Papadopoulos, R. R. Penman, L. Qian, J. J. Rocca, A. A. Shaykin, C. W. Siders, C. Spindloe, S. Szatmári, R. M. G. M. Trines, J. Zhu, P. Zhu, and J. D. Zuegel, Petawatt and exawatt class lasers worldwide, *High Power Laser Science and Engineering* **7**, e54 (2019).
- [23] M. J. Quin, *Coherence Effects and Spin Polarisation of Electrons in Electromagnetic Fields*, Master's thesis, University of Heidelberg (2020).
- [24] M. J. Quin, *Classical Radiation Reaction and Collective Behaviour*, Ph.D. thesis, University of Heidelberg (2023).
- [25] E. Gelfer, A. Fedotov, O. Klimo, and S. Weber, Coherent radiation of electrons in an intense laser pulse (2023), [arXiv:2306.16945](https://arxiv.org/abs/2306.16945) [physics.plasm-ph].
- [26] G. Sarri, K. Poder, J. M. Cole, W. Schumaker, A. di Piazza, B. Reville, T. Dzelzainis, D. Doria, L. A. Gizzi, G. Grittani, S. Kar, C. H. Keitel, K. Krushelnick, S. Kuschel, S. P. D. Mangles, Z. Najmudin, N. Shukla, L. O. Silva, D. Symes, A. G. R. Thomas, M. Vargas, J. Vieira, and M. Zepf, Generation of neutral and high-density electron-positron pair plasmas in the laboratory, *Nat. Commun.* **6**, 6747 (2015).
- [27] C. D. Arrowsmith, P. Simon, P. J. Bilbao, A. F. A. Bott, S. Burger, H. Chen, F. D. Cruz, T. Davenne, I. Efthymiopoulos, D. H. Froula, A. Goillot, J. T. Gudmundsson, D. Haberberger, J. W. D. Halliday, T. Hodge, B. T. Huffman, S. Iaquinta, F. Miniati, B. Reville, S. Sarkar, A. A. Schekochihin, L. O. Silva, R. Simpson, V. Stergiou, R. M. G. M. Trines, T. Vieu, N. Charitonidis, R. Bingham, and G. Gregori, Laboratory realization of relativistic pair-plasma beams, *Nat. Commun.* **15**, 5029 (2024).
- [28] H. Chen, S. C. Wilks, D. D. Meyerhofer, J. Bonlie, C. D. Chen, S. N. Chen, C. Courtois, L. Elberson, G. Gregori, W. Kruer, O. Landoas, J. Mithen, J. Myatt, C. D. Murphy, P. Nilson, D. Price, M. Schneider, R. Shepherd, C. Stoeckl, M. Tabak, R. Tommasini, and P. Beiersdorfer, Relativistic quasisimonoenergetic positron jets from intense laser-solid interactions, *Phys. Rev. Lett.* **105**, 015003 (2010).
- [29] H. Chen and F. Fiúza, Perspectives on relativistic electron-positron pair plasma experiments of astrophysical relevance using high-power lasers, *Phys. Plasmas* **30**, 020601 (2023).
- [30] F. Rohrlich, *Classical Charged Particles*, 3rd ed. (World Scientific, 2007).
- [31] A. Di Piazza, C. Müller, K. Z. Hatsagortsyan, and C. H. Keitel, Extremely high-intensity laser interactions with fundamental quantum systems, *Rev. Mod. Phys.* **84**, 1177 (2012).
- [32] A. Gonoskov, T. G. Blackburn, M. Marklund, and S. S. Bulanov, Charged particle motion and radiation in strong electromagnetic fields, *Rev. Mod. Phys.* **94**,



- 045001 (2022).
- [33] A. Fedotov, A. Ilderton, F. Karbstein, B. King, D. Seipt, H. Taya, and G. Torgrimsson, Advances in qed with intense background fields, *Physics Reports* **1010**, 1 (2023).
- [34] M. J. Quin, A. D. Piazza, C. H. Keitel, and M. Tamburini, Interparticle-fields amplified radiation reaction (2023), [arXiv:2306.17832 \[physics.plasm-ph\]](https://arxiv.org/abs/2306.17832).
- [35] L. D. Landau and E. M. Lifshitz, *The Classical Theory of Fields*, 2nd ed. (Elsevier, Oxford, 1975).
- [36] M. Tamburini, F. Pegoraro, A. Di Piazza, C. H. Keitel, and A. Macchi, Radiation reaction effects on radiation pressure acceleration, *New J. Phys.* **12**, 123005 (2010).
- [37] J. D. Jackson, *Classical Electrodynamics*, 3rd ed. (John Wiley and Sons, Inc., 1998).
- [38] S. Y. Mironov, V. N. Ginzburg, V. V. Lozhkarev, G. A. Luchinin, A. V. Kirsanov, I. V. Yakovlev, E. A. Khazanov, and A. A. Shaykin, Highly efficient second-harmonic generation of intense femtosecond pulses with a significant effect of cubic nonlinearity, *Quantum Electron.* **41**, 963 (2011).
- [39] Y. Wang, S. Wang, A. Rockwood, B. M. Luther, R. Hollinger, A. Curtis, C. Calvi, C. S. Menoni, and J. J. Rocca, 0.85 PW laser operation at 3.3 Hz and high-contrast ultrahigh-intensity  $\lambda = 400$  nm second-harmonic beamline, *Opt. Lett.* **42**, 3828 (2017).
- [40] S. Y. Mironov, V. N. Ginzburg, V. V. Lozhkarev, G. A. Luchinin, A. V. Kirsanov, I. V. Yakovlev, E. A. Khazanov, and A. A. Shaykin, Highly efficient second-harmonic generation of intense femtosecond pulses with a significant effect of cubic nonlinearity, *Quantum Electron.* **41**, 963 (2011).
- [41] R. R. Almeida and J. Vieira, private communication (2023).
- [42] C. Erciyas, private communication (2024).
- [43] *FLASH1 – Free Electron Laser* (2024).
- [44] J. Duris, S. Li, T. Driver, E. G. Champenois, J. P. MacArthur, A. A. Lutman, Z. Zhang, P. Rosenberger, J. W. Aldrich, R. Coffee, G. Coslovich, F.-J. Decker, J. M. Glowia, G. Hartmann, W. Helml, A. Kamalov, J. Knurr, J. Krzywinski, M.-F. Lin, J. P. Marangos, M. Nantel, A. Natan, J. T. O’Neal, N. Shivaram, P. Walter, A. L. Wang, J. J. Welch, T. J. A. Wolf, J. Z. Xu, M. F. Kling, P. H. Bucksbaum, A. Zholents, Z. Huang, J. P. Cryan, and A. Marinelli, Tunable isolated attosecond x-ray pulses with gigawatt peak power from a free-electron laser, *Nat. Photonics* **14**, 30 (2020).
- [45] X. Ren, J. Li, Y. Yin, K. Zhao, A. Chew, Y. Wang, S. Hu, Y. Cheng, E. Cunningham, Y. Wu, M. Chini, and Z. Chang, Attosecond light sources in the water window, *J. Opt.* **20**, 023001 (2018).
- [46] T. Gaumnitz, A. Jain, Y. Pertot, M. Huppert, I. Jordan, F. Ardana-Lamas, and H. J. Wörner, Streaking of 43-attosecond soft-x-ray pulses generated by a passively cep-stable mid-infrared driver, *Opt. Express* **25**, 27506 (2017).
- [47] F. Silva, S. M. Teichmann, S. L. Cousin, M. Hemmer, and J. Biegert, Spatiotemporal isolation of attosecond soft x-ray pulses in the water window, *Nat. Commun.* **6**, 6611 (2015).
- [48] C. Spielmann, N. H. Burnett, S. Sartania, R. Koppitsch, M. Schnürer, C. Kan, M. Lenzner, P. Wobrauschek, and F. Krausz, Generation of coherent x-rays in the water window using 5-femtosecond laser pulses, *Science* **278**, 661 (1997).
- [49] Y. I. Salamin, G. R. Mocken, and C. H. Keitel, Electron scattering and acceleration by a tightly focused laser beam, *Phys. Rev. ST Accel. Beams* **5**, 101301 (2002).
- [50] M. Abramowitz and I. Stegun, *Handbook of Mathematical Functions with Formulas, Graphs, and Mathematical Tables* (1968).

## Acknowledgements

This article comprises part of the PhD work of Michael J. Quin, which was successfully defended at Heidelberg University on the 18th of October, 2023. The authors wish to thank Rafael R. Almeida, Çağrı Erciyas, Gianluca Aldo Geloni, Anna Golinelli, Christian Ott, Thomas Pfeifer, Brian Reville, Gianluca Sarri, and Jorge Vieira for helpful discussions.

## Author Contributions

The idea for this paper originated with M.J.Q., A.D.P. and M.T. Code development, simulations and data analysis were performed by M.J.Q with oversight by M.T. Interpretation and theoretical work were performed by M.J.Q., A.D.P. and M.T., with oversight from C.H.K. The manuscript was written by M.J.Q., A.D.P. and M.T., with contributions from C.H.K.

## Competing interests

The authors declare no competing interests.